*Optica Applicata, Vol. XLIV, No. 1, 2014*
DOI: 10.5277/oa140112

# The role of quantum-well states and carrier scattering times in discontinuities of opto-electrical characteristics of SCH lasers

ZBIGNIEW KOZIOŁ[1*], SERGEY I. MATUKHIN[1], EVGENIYA A. BUDULEVA[2]

[1] State University – Education-Science-Production Complex,
29 Naugorskoye Shosse, Oryol, 302020, Russia

[2] Oryol State University, 95 Komsomolskaya Street, Oryol, 302026, Russia

[*] Corresponding author: zbigniew@ostu.ru

Drift-diffusion computer simulation model available in Synopsys' *Sentaurus TCAD User Guide* is used to study electrical and optical characteristics of a separate-confinement heterostructure laser based on AlGaAs. We investigate the role of the width and depth of quantum-well active region, below and above the lasing threshold. The device properties depend on both, the number of bound quantum-well states and on closeness of the highest bound states to conduction or valence band offset. The lasing action may not exist at certain widths or depths of quantum-well, and the threshold current is a discontinuous function of these parameters, at such values of quantum-well width or depth when the highest quantum-well bound states cross conduction or valence band energy offset. The effects are more pronounced at low temperatures. Discontinuities in characteristics are found, at certain conditions, in temperature dependences as well. The carriers scattering time on quantum-well is shown to have a crucial role for the amplitude of discontinuities of these characteristics. The current below the lasing threshold and the threshold current density itself decrease with an increase of quantum-well scattering times and the amplitude of discontinuities decreases then as well.

Keywords: SCH laser, quantum-well, heterostructure, carrier scattering time, AlGaAs, discontinuous *I–V* characteristics.

## 1. Introduction

Computer modeling of electronic devices is a relatively new, rapidly developing approach towards the study of physical phenomena occurring there as well as optimizing their technical characteristics. Methodologically, this field of scientific and engineering activity may be placed between theory and experiment, not replacing either of them: pursuing research of that kind requires theoretical understanding of physics of

microscopic processes and may work as a helpful tool in interpretation of experimental data. In some situations, results of that research may provide an inspiration for understanding or testing physical phenomena: it is easier, faster and less expensive to perform modeling than experiments, and we are not restricted that much by, often large, inaccuracy of experimental data that may hide insightful details.

One of the main problems in the field of semiconductor laser devices is minimization of the threshold current density required to achieve spontaneous laser action. That current depends on a number of factors, material specific and geometric. Among the others, the width and depth of a quantum-well (QW) and time of carriers capture in bound QW states are important and investigated extensively.

When performing modeling AlGaAs SCH lasers with Synopsys' *Sentaurus TCAD User Guide* [1], we noticed unexpected steps in some of their characteristics (threshold current $I_{\mathrm{th}}$ *vs.* the width of QW $d_a$ [2, 3], or *vs.* its depth, *etc.*). Analyses of results led us to the conclusion that observed discontinuities occur when the most upper bound QW state crosses the conduction or valance band offset energy. Following that idea, we performed modeling showing that the effects ought to manifest themselves in discontinuities of characteristics below the lasing offset, which should be present in curves for gain (or loss) *vs.* current. Moreover we expect the discontinuites in the temperature dependences of physical quantities (*e.g.*, in *I–V* characteristics) if laser parameters are chosen properly. In this work we show the crucial role of QW carrier scattering times for these observations.

## 2. Modeling

### 2.1. Reproducing experimental results

The laser we are modeling has dimensions, structure and doping as described by ANDREEV *et al.* [4, 5]. The lasing wavelength is 808 nm, the lasing offset voltage $U_0$ is 1.56–1.60 V, differential resistance just above the lasing offset $r = \mathrm{d}U/\mathrm{d}I$ is 50–80 mΩ, threshold current $I_{\mathrm{th}}$ is 200–300 mA, slope of optical power $S = \mathrm{d}L/\mathrm{d}I$ is 1.15–1.25 W/A. The reference laser has the width of QW, $d_a$, of 12 nm and both waveguides' width is 0.2 μm.

In order to reproduce the above laser characteristics in computational results, we played with several adjustable variables available in [1, 3]. Important in this case are these related to light absorption and carrier scattering. Experiments show that the absorption coefficient is of the order of $\mathrm{cm}^{-1}$ [4]. It is argued that in AlGaAs lasers the main contribution to a light absorption coefficient is due to photon scattering on free carriers $\alpha_{\mathrm{fc}}$ and it is given by $\alpha_{\mathrm{fc}} = (\alpha_n n + \alpha_p p)$, where $n$ and $p$ are the electron and hole density. We choose in our calculations such values of $\alpha_n$ and $\alpha_p$ that an effective absorption coefficient obtained is close to the experimental one.

It is important also to have a reasonable value of a radiative recombination rate $R_r$, which is assumed to be described by $R_r = C(np - n_{\mathrm{ieff}}^2)$, where $n_{\mathrm{ieff}}$ describes the effective intrinsic density, and $C$ is a parameter available for changes.

## 2.2. Typical characteristics: steps in $I(d_a)$

Typical $I$–$V$ characteristics computed at $T = 300$ K are shown in Fig. 1, for a broad range of QW widths. For current near but below the lasing threshold current $I_{\rm th}$ (*i.e.*, for voltage near the lasing offset voltage $U_0$), which corresponds to a kink in $I$–$V$, for most of these curves the results are very well approximated by a modified exponential relation [6], $I(U) = I_{\rm th}\exp(A(U - U_0) + B(U - U_0)^2)$, where $A$, $B$ are certain fitting parameters, with values of $A$ and $B$ being different below and above lasing threshold.

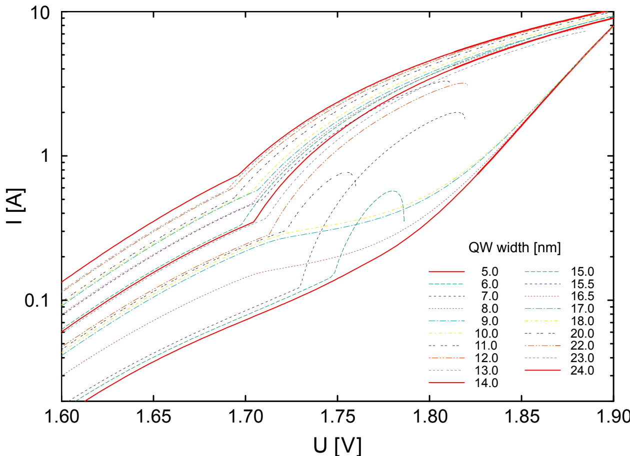


Fig. 1. Typical $I$–$V$ characteristics computed at $T = 300$ K. OpticalLoss parameter is assumed 0, no radiative recombination, free carrier scattering rate parameters $\tau_n$ and $\tau_p$ are $8.0\times10^{-13}$ and $4.0\times10^{-13}$ s$^{-1}$, with electron and hole mobilities 9200 and 400 cm$^2$V$^{-1}$s$^{-1}$. The legend describes the width of QW (in nm), from 5 for right-bottom curve to 24 nm for uppermost curve.

A straightforward quantitative interpretation of these curves around the lasing threshold is not possible, since we deal here with a strong, nonlinear interplay between the effects of carrier transport and scattering, light absorption, recombination, lasing action, *etc*. However, we may notice an interesting feature: while the width of QW changes (nearly) monotonically in Fig. 1, the curves are grouped into a few sets such that they nearly coincide, within each group.

A very similar feature is observed when the gain or loss are drawn as a function of current, for many widths of an active region.

Therefore, we conclude that below the lasing threshold, the current as a function of QW width at constant voltage, derived from data like these in Fig. 1, or the gain or the loss as a function of QW width, at constant current values, also below the lasing threshold, will follow step-like functions.

This is illustrated in Fig. 2, where the current as a function of QW width, derived at constant voltage from data curves similar to these as in Fig. 1, is shown. Figure 2 presents data computed at different conditions, and marked from $A$ to $F$, for several combinations of free carrier scattering coefficients, $\alpha_n$ and $\alpha_p$, and values of $C$,

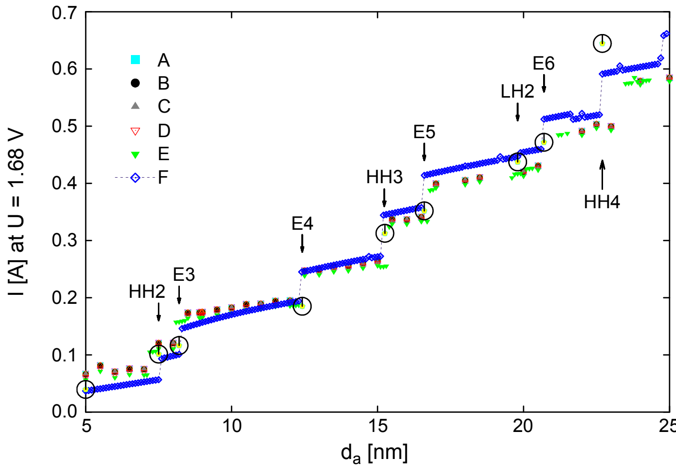


Fig. 2. Current as a function of QW width derived at constant voltage from data curves as these shown in Fig. 1, for QW carrier scattering parameters as described in Table 1. The solid line for data points *F* is to guide the eyes, only. *F* is computed for constant Al concentration in QW of 8%, while all other datasets (*A–E*) are computed with such a concentration of Al in QW that lasing wavelength will remain constant (808 nm) when QW width changes. The arrows are for data points *F*. From the results of a separate analysis, it follows that the relative height of steps and the position of these steps do not depend on voltage at which current is measured, even though current values may change as much as 100 times.

the radiative recombination parameter, as described in Table 1. Dataset *F* differs from datasets *A–E*. The last ones are computed assuming changing Al concentration in waveguides (when Al in QW is kept constant) in such a way that the lasing wavelength does not change with the change of QW width, while the dataset *F* is computed for constant Al concentration in waveguides of 33%. Hence, in case of dataset *F* we do not care that lasing wavelength changes slightly during the change in QW width, while in cases *A–E* we adjust Al concentration in QW in such a way during QW width change that lasing wavelength remains constant at 808 nm. The solid line in Fig. 2 is drawn

Table 1. A few sets of simulation conditions (*A–F*) for data shown in Fig. 2. Parameter *C* is the radiative recombination rate, and $\alpha_n$, $\alpha_p$ are the coefficients of free carrier absorption equation. Temperature for all cases is 300 K, electron and hole scattering times are assumed $8.0\times10^{-13}$ and $4.0\times10^{-13}$ s$^{-1}$, respectively, and electron and hole mobility are 9200 and 400 cm$^2$V$^{-1}$s$^{-1}$, respectively. No additional light scattering mechanisms are considered.

| | $C$ [cm$^3$s$^{-1}$] | $\alpha_n$ [cm$^{-2}$] | $\alpha_p$ [cm$^{-2}$] |
|---|---|---|---|
| *A* | $2.0\times10^{-10}$ | $1.0\times10^{-18}$ | $2.0\times10^{-18}$ |
| *B* | $2.0\times10^{-10}$ | $5.0\times10^{-17}$ | $1.0\times10^{-18}$ |
| *C* | $2.0\times10^{-10}$ | $1.5\times10^{-18}$ | $3.0\times10^{-18}$ |
| *D* | $1.0\times10^{-10}$ | $1.5\times10^{-18}$ | $3.0\times10^{-18}$ |
| *E* | 0 | $1.5\times10^{-18}$ | $3.0\times10^{-18}$ |
| *F* | 0 | $1.5\times10^{-18}$ | $3.0\times10^{-18}$ |

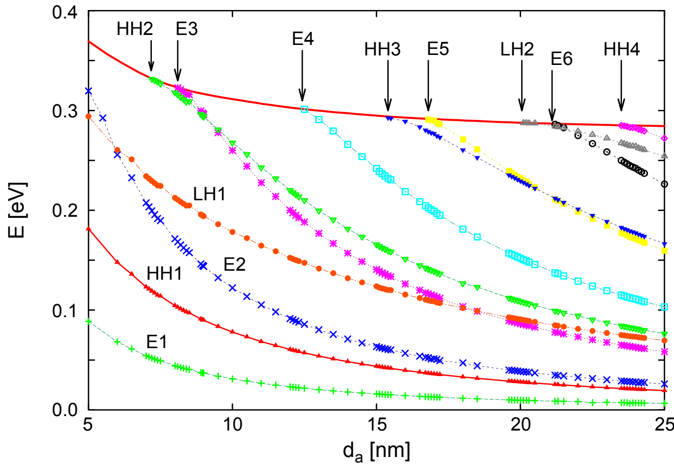


Fig. 3. Conduction and valence band offset energy ($E_{CBO}$ and $E_{VBO}$; solid line), and electron $E_n$, light- and heavy-hole energies ($LH_n$ and $HH_n$) in QW, as a function of QW width, computed at $T = 300$ K. Hole energies and $E_{VBO}$ have been scaled up by a factor 28 to obtain coincidence with an electron energy scale (*i.e.*, that $E_{CBO}$ and $E_{VBO}$ curves are the same in this figure).

through data-points $F$, and arrows there refer to curve $F$ as well, and indicate positions of bound QW energy states crossing the conduction or valance band offset energies. Positions of bound QW energy states for cases $A$–$E$ are very close to but not identical to these for curve $F$. The results of Fig. 3, described in more details earlier [7], were also found to be exactly the same as those computed by using nextnano software [8].

The step-like features are preserved also in $I_{th}(d_a)$ dependences. Changes in QW depth (caused by differences in Al concentration in QW and waveguides) cause very similar step-like dependences. The effects are in some situations more clear and pronounced at low temperatures, as confirmed by modeling for $T = 77.6$ K [7].

## 2.3. Discontinuities in $I(T)$

With a careful design of laser structure (content of Al in QW and waveguides) it is possible to find the evidence of the effect described in temperature dependence of current, when measurements are performed at constant voltage. Temperature dependence of energy gap in AlGaAs is well approximated by a parabolic Varshni expression [9], which is used by Synopsys. However, Al concentration in waveguide is different than in QW and that results also in a parabolic dependence of QW depth but with a minimum at around 250 K. Hence, in some cases, a crossing of uppermost QW bound states of $E_{CBO}$ should occur when temperature is changed.

We found such Al concentrations when the number of QW bound states changes with temperature sweep [7]. An example of $I(T)$ dependences, for carefully chosen three values of Al content in waveguide, is shown in Fig. 4. There, results are shown for three values of voltage applied, all below the lasing threshold. The lines in this fig-

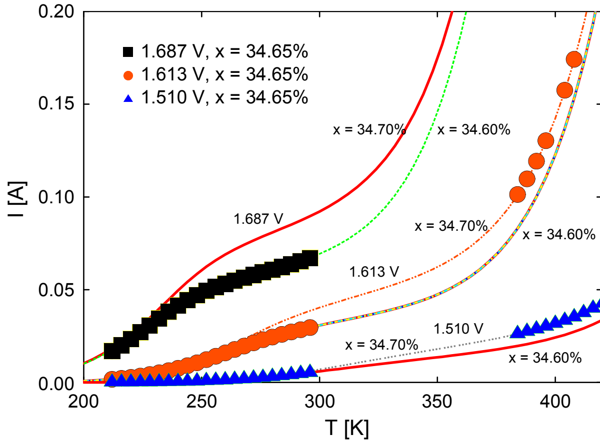


Fig. 4. Temperature dependence of current for three values of voltage applied (1.510, 1.613, and 1.687 V; for each it is below the lasing threshold), and for three values of Al concentrations in waveguide.

ure are drawn for two values of Al content, 34.60% and 34.70%, that are very close to but slightly different than results represented by data points (in all cases Al concentration in QW is 8%). In case of these both Al concentrations, the number of bound QW states does not change with temperature, and it is different in both cases: at 34.60% of Al, there are 3 bound electron states in QW, while at 34.70% of Al there are 4 of them. At 34.65% of Al, the number of bound electron states in QW changes during temperature sweep. In case of that concentration, initially, at low temperatures current values obtained follow the curve for 34.60% of Al (there are 3 bound electron states), then there is a gap (we were not able to achieve convergence of computation when the uppermost bound QW level is very close to $E_{\mathrm{CBO}}$) and next the data points follow the curve computed for 34.70% of Al (there are 4 bound electron states).

For Al concentration 34.70%, the $E_4$ energy level exists always through temperature sweep studied. For Al concentration 34.65%, the $E_4$ energy level does not exist bellow around 300 K. For Al concentration 34.60%, the $E_4$ energy level does not exist in the temperature range shown in Fig. 4.

We expect that similar effects, due to crossing of conduction band offset energy by bound QW states should manifest themselves also in measurements performed under uniaxial or hydrostatic pressure.

## 3. The role of QW scattering times

The modeling results reported above were computed by using default (in *Sentaurus TCAD User Guide*) values of the parameters related to carriers scattering times on QW (*i.e.*, time of living of carriers in bound QW states, QweScatTime and QwhScatTime, with their physical meaning explained more precisely in Section 4.3). An approach

used in *Sentaurus TCAD User Guide* is to have constant values of these parameters (which however may be adjusted by the user).

Existing theoretical and other computational results indicate that carriers scattering times depend on QW width [10, 11]. Scattering on longitudinal optical phonons, LO, is considered as the main mechanism [12]. BIRNER [11] computed the lifetime of electron bound on to the given energy state for transitions between the initial state $E_2$ and the final ground state $E_1$), *i.e.*, for an intersubband transition, for different QW widths, at $T = 0$.

The nextnano[3] calculations of BIRNER [11] are in a good agreement with these of FERREIRA and BASTARD [10]. For QW widths smaller than about 5.4 nm, only the ground state is confined and $E_2$ is unbound. For QW widths larger than about 18 nm, the transition energy becomes smaller than the LO phonon energy and scattering through the emission of an LO phonon is not possible any more (scattering on carriers will dominate then).

In order to have a better view on what is the effect of scattering times on the amplitude of steps (and their existence) in opto-electrical characteristics of the device, we performed simulations for several sets of values of parameters available in [1].

Typical results are shown in Fig. 5. Shorter QW scattering times lead to a strong increase in current and pronounced steps in the current as a function of QW width. We observed that the value of parameters eQWMobility and hQWMobility available in [1] has no noticeable effects on these results.

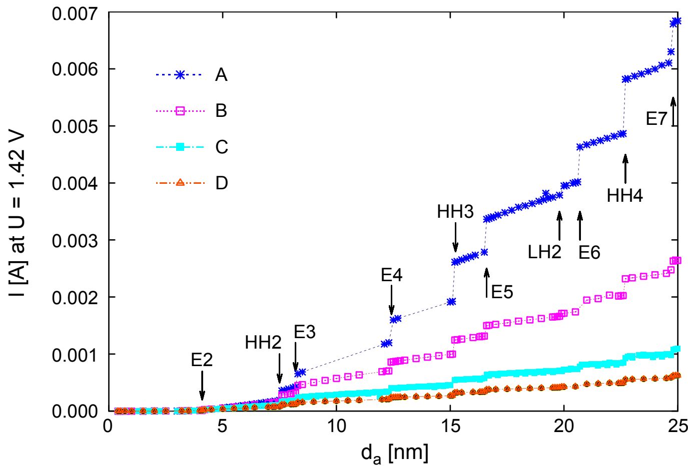


Fig. 5. The effect of QW scattering times on current at a constant voltage as a function of QW width. The data were obtained by using the same values of parameters eQWMobility and hQWMobility, 9200 and 400 $cm^2V^{-1}s^{-1}$, respectively (the results do not depend in a noticeable manner on the value of these parameters, even when they are increased or decreased by a factor of 10). The following sets of (QWeScatTime, QWhScatTime) were used, for curves *A* to *D* (from top to bottom): $(1\times10^{-13}, 5\times10^{-14})$, $(8\times10^{-13}, 4\times10^{-13})$, $(4\times10^{-12}, 2\times10^{-12})$, and $(1\times10^{-11}, 5\times10^{-12})$, where time is in seconds.

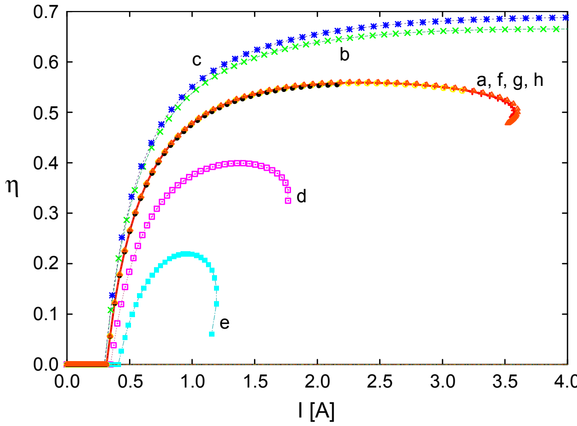


Fig. 6. Optical efficiency, $L/UI$ for a laser with 12 nm QW width. The data were obtained by using the same values of parameters eQWMobility and hQWMobility, 9200 and 400 $cm^2V^{-1}s^{-1}$, respectively, (the results do not depend in a noticeable manner on the value of these parameters, even when they are increased or decreased by a factor of 10). The following sets of (QWeScatTime, QWhScatTime) were used, for curves *a* to *e*: ($1\times10^{-13}$, $5\times10^{-14}$), ($2\times10^{-13}$, $2\times10^{-13}$), ($8\times10^{-13}$, $4\times10^{-13}$), ($2\times10^{-12}$, $2\times10^{-12}$), and ($4\times10^{-12}$, $2\times10^{-12}$), where time is in seconds. In case of curves *f* to *h* (QWeScatTime, QwhScatTime) parameters are the same as for curves *a* to *e* except that sets of (eQWMobility, hQWMobility) parameters change to (5000, 200), (1000, 40), and (20000, 800) $cm^2V^{-1}s^{-1}$, respectively.

As an illustration, we show also optical efficiency curves (Fig. 6) for a few sets of values of QW scattering parameters, where the role of QW scattering for opto-electrical characteristics of a device is evident (these modeling results are in a qualitative agreement with theory and experiment [13]).

## 4. Discussion

### 4.1. Tunneling through energy barrier

In case of tunneling through an energy barrier, a transfer matrix approach is used to describe charge transport through it [14, 15]. The interband tunneling current is:

$$J \propto \int_{E_{\min}}^{E_{\max}} N(E) f(E) T(E) \mathrm{d}E \tag{1}$$

where $T(E)$ is the energy-dependent tunneling rate, $N(E)$ is the density of states, $f(E)$ is the Fermi–Dirac distribution function, and $E_{\min}$ and $E_{\max}$ are minimum and maximum carrier energies available.

### 4.2. Drift-diffusion scattering

In *Sentaurus TCAD User Guide*, a simplified intuitive model is used to handle the physics of carrier scattering at the QW. The carrier populations are separated into bound

and continuum states, and separate continuity equations are applied to both populations. The QW scattering model accounts for the net capture rate, that is, not all of the carriers will be scattered into the bound states of the QW. The electron capture rate from the continuum (subscript $c$) to the bound (subscript $b$) states is:

$$R = \int_{E_c}^{\infty} \mathrm{d}E_c \int_{E_b}^{\infty} \mathrm{d}E_b\, N_c(E_c) N_b(E_b) S(E_b, E_c) f_c(E_c) \left[1 - f_b(E_b)\right] \tag{2}$$

where $E_c$ and $E_b$ are the energy levels of lowest conduction band and bound QW electron states, $N(E)$ is the density-of-states, $S(E_b, E_c)$ is the scattering probability. The reverse process gives the electron emission rate from the bound to continuum states:

$$M = \int_{E_c}^{\infty} \mathrm{d}E_c \int_{E_b}^{\infty} \mathrm{d}E_b\, N_c(E_c) N_b(E_b) S(E_b, E_c) f_b(E_b) \left[1 - f_c(E_c)\right] \tag{3}$$

The net capture rate is $C = R - M$, and for very deep QWs is known to be given by approximation:

$$C = R - M = \left[1 - \exp(\eta_b - \eta_c)\right] \frac{n_c}{\tau} \tag{4}$$

where $\eta_b = (-q\Phi_b - E_c)/k_B T$ and $\eta_c = (-q\Phi_c - E_c)/k_B T$ contain the quasi-Fermi level information and $\tau$ is the capture time.

### 4.3. Scattering times

The capture time represents scattering processes attributed to carrier–carrier and carrier–LO phonon interactions involving bound QW states (of which, it is generally assumed, carrier–LO phonon is dominating in the case considered). The net capture rate $C$ is added to the continuity equations as a recombination term. In a similar way, the scattering of holes is treated, with their own characteristic capture time. These parameters are specified in *Sentaurus TCAD User Guide* by the keywords QWeScatTime and QWhScatTime. Their default values, $8\times10^{-14}$ and $4\times10^{-13}$ s, respectively, correspond reasonably well to these based on theory [16, 17], while photoluminescence spectroscopy results give values of an order of 3–20 ps [17]. In most of our modeling, if not indicated otherwise, we use also the default values of electron and hole mobility, represented in *Sentaurus TCAD User Guide* by parameters eQWMobility = = 9200 $\mathrm{cm^2V^{-1}s^{-1}}$ and hQWMobility = 400 $\mathrm{cm^2V^{-1}s^{-1}}$, since we do not observe a noticeable changes of $I$–$V$–$L$ laser characteristics when these parameters increase or decrease a few times.

It should be pointed out that Eqs. (2)–(4), while provide a convenient, intuitive description of carriers scattering and capture on QW, are approximate only. In particular, there is no dependence of capture time on the energy of unbound carriers there and no observed sometime quasi-periodic oscillations as a function of QW size [16, 17].

### 4.4. Density of bound states

Equations (1)–(3) all depend on the density of bound states in QW. We expect hence that the current through the QW is proportional to the density of all bound states in QW. In effective mass approximation, the two-dimensional density of electron states within each QW subband $n$ equals (for $E > E_n$) [15]:

$$N_n(E) = \frac{m_n}{\pi h^2} \tag{5}$$

Hence, the current should be proportional to the (number of bound states)×(carrier mass). The quantity computed this way (with a certain multiplication factor) is represented by large circles in Fig. 2. Though it need not to be exact (for instance, no difference in scattering rates for electrons and holes is accounted for), it fits reasonably well the $I(d_a)$ dependence.

In our modeling, we assumed scattering times independent of QW width (modeling is performed however for a few sets of scattering times). In BIRNER [11] and FERREIRA and BASTARD [10] results, scattering time steeply increases with a decrease in QW width, below the width of around 6 nm, and slowly, monotonically decreases when it becomes larger that about 6 nm, with a value of around $10^{-12}$ s at 7 nm.

The default value of scattering time used by *Sentaurus TCAD User Guide* is $8\times10^{-13}$ s, for electrons. That suggests that results represented by data on curves $B$ and $C$ in Fig. 5 should be closest to these expected experimentally. At the same time, changing of scattering times with QW width should not diminish the existence of steps since these changes are monotonic. Also, the steps should become more pronounced at large QW widths, as well the current values should increase in a steeper way than would follow from Figs. 2 or 5. It ought however to be remembered that in Birner's example results [11], electrons scattering only is taken into account and only transitions between the lowest bound electron states. The results reported in literature often predict a quasi-periodic dependence of scattering times on QW width [16–18].

## 5. Summary and conclusions

When modeling the laser characteristics as a function of the width of active region, a non-monotonic, discontinuous dependence of $I(d_a)$ (when measured at constant voltage applied) was found. A careful analysis of the data led us to the hypothesis that discontinuities occur when the most upper QW, bound energy states are found very close to the conduction or valence band energy offsets. The effect, hence, is thought to be related to changes in the density of states of carriers from the one hand, and to fast changes in carrier transfer through QW for QW bound states close to $E_{\mathrm{CBO}}$ or $E_{\mathrm{VBO}}$. As such, it ought to be more pronounced at lower temperatures, as confirmed by the results of our earlier modeling $I(d_a)$ at low temperatures.

The effect is observed also when modeling the current as a function of QW depth (Al concentration in waveguide).

There is no experimental evidence, so far, of the existence of similar effects. This may be due to difficulties in performing similar measurements with the accuracy required for their observation (the main difficulty is creating a large number of devices with a broad range of well controlled width or depth of QWs). However, we argue that a similar effect will be present also in modeling $I$ as a function of temperature for the samples where a careful design of laser properties is prepared in such a way that a transition of the most upper QW energy state will pass through an edge of QW when temperature is swept. As well, we expect also that performing measurements on laser devices under uniaxial or hydrostatic pressure might provide an experimental evidence on the significance of these effects in real devices.

These observations are potentially important for proper designing of semiconducting lasers (choice of Al concentrations, thickness of the active region, *etc*.), and, potentially, might be useful for designing a kind of quantum level spectroscopy tool for testing lasers for technological applications.

This work is restricted to discussing the properties of AlGaAs heterostructures. An open question is how significant are the effects described in case of other materials.

*Acknowledgements* – We are indebted to A.A. Marmalyuk of "Polyus" Research and Development Institute in Moscow for valuable critical comments and discussions.

## References

[1] *Sentaurus TCAD User Guide*, Synopsys, 2010, http://www.synopsys.com

[2] Matyukhin S.I., Koziol Z., *Influence of the active region width on characteristics of AlGaAs semiconductor laser with separate confinement heterostructures*, Nanoengineering **5**, 2012, p. 14, (in Russian).

[3] Koziol Z., *Quantum-well states and discontinuities in opto-electrical characteristics of SCH lasers*, arXiv:1112.0139v1 [cond-mat.mtrl-sci], 2011.

[4] Andreev A.V., Leshko A.Y., Lyutetskiy A.V., Marmalyuk A.A., Nalyot T.A., Padalitsa A.A., Pikhtin N.A., Sabitov D.R., Simakov V.A., Slipchenko S.O., Khomylev M.A., Tarasov I.S., *High-power laser diodes ($\lambda$ = 808–850 nm) based on asymmetric separate-confinement heterostructures*, Semiconductors **40**(5), 2006, pp. 611–614.

[5] Andreev A.Yu., Zorina S.A., Leshko A.Yu., Lyutetskiy A.V., Marmalyuk A.A., Murashova A.V., Nalet T.A., Padalitsa A.A., Pikhtin N.A., Sabitov D.R., Simakov V.A., Slipchenko S.O., Telegin K.Yu., Shamakhov V.V., Tarasov I.S., *High-power lasers ($\gamma$ = 808 nm) based on the AlGaAs/GaAs heterostructures of separate confinement*, Semiconductors **43**(4), 2009, pp. 519–523.

[6] Koziol Z., Matyukhin S.I., *Modified exponential I(U) dependence and optical efficiency of AlGaAs SCH lasers in computer modeling with Synopsys TCAD*, arXiv:1107.4668v1 [cond-mat.mtrl-sci], 2011.

[7] Koziol Z., Matyukhin S.I., *The lasing wavelength of QW active region of AlGaAs SCH lasers*, Romanian Journal of Physics **57**(3–4), 2012, pp. 711–719.

[8] Birner S., Zibold T., Andlauer T., Kubis T., Sabathil M., Trellakis A., Vogl P., *Nextnano: general purpose 3-D simulations*, IEEE Transactions on Electron Devices **54**(9), 2007, pp. 2137–2142.

[9] Varshni Y.P., *Temperature dependence of the energy gap in semiconductors*, Physica **34**(1), 1967, pp. 149–154.

[10] Ferreira R., Bastard G., *Evaluation of some scattering times for electrons in unbiased and biased single- and multiple-quantum-well structures*, Physical Review B **40**(2), 1989, pp. 1074–1086.

[11] BIRNER S., *Nextnano$^3$ – Tutorial. Scattering Times for Electrons in Unbiased and Biased Single and Multiple Quantum Wells*, http://www.nextnano.de

[12] POZHELA YU., POZHELA K., YUTSENE V., SUZHEDELIS A., SHKOL'NIK A.S., MIKHRIN S.S., MIKHRIN V.S., *Vzaimodeystviye elektronov s lokalizovannymi v kvantovoy yame opticheskimi fononami*, Fizika i Tekhnika Poluprovodnikov **43**(12), 2009, pp. 1634–1640, (in Russian).

[13] SOKOLOVA Z.N., TARASOV I.S., ASRYAN L.V., *Zakhvat nositeley zaryada i vykhodnaya moshchnost' lazera na kvantovoy yame*, Fizika i Tekhnika Poluprovodnikov **45**(11), 2011, pp. 1553–1559, (in Russian).

[14] DAVIES J.H., *The Physics of Low-Dimensional Semiconductors. An Introduction*, Cambridge University Press, 1998.

[15] PIPREK J., *Semiconductor Optoelectronic Devices. Introduction to Physics and Simulation*, Academic Press, 2003.

[16] HERNÁNDEZ-ROSAS J., VILLEGAS-LELOVSKY L., GONZÁLEZ DE LA CRUZ G., *Capture of carriers by quantum wells via optical-phonon deformation potential*, Revista Mexicana de Física **48**(4), 2002, pp. 295–299.

[17] BLOM P.W.M., SMITH C., HAVERKORT J.E.M., WOLTER J.H., *Carrier capture into a semiconductor quantum well*, Physical Review B **47**(4), 1993, pp. 2072–2081.

[18] MOSKO M., KÁLNA K., *Carrier capture into a GaAs quantum well with a separate confinement region: comment on quantum and classical aspects*, Semiconductor Science and Technology **14**(9), 1999, pp. 790–796.

*Received May 19, 2013*
*in revised form July 10, 2013*